Fsp27 promotes lipid droplet growth by lipid exchange and transfer at lipid droplet contact sites

Jingyi Gong,[1] Zhiqi Sun,[1] Lizhen Wu,[1] Wenyi Xu,[1] Nicole Schieber,[2,3] Dijin Xu,[1] Guanghou Shui,[4] Hongyuan Yang,[5] Robert G. Parton,[2,3] and Peng Li[1]

[1]Peking-Tsinghua Center for Life Sciences, Tsinghua University, Beijing 100084, China
[2]Institute for Molecular Bioscience and [3]Centre for Microscopy and Microanalysis, University of Queensland, Brisbane 4072, Australia
[4]Life Sciences Institute, National University of Singapore, Queenstown, Singapore 119077
[5]School of Biotechnology and Biomolecular Sciences, University of New South Wales, Sydney NSW 2052, Australia

Lipid droplets (LDs) are dynamic cellular organelles that control many biological processes. However, molecular components determining LD growth are poorly understood. Genetic analysis has indicated that Fsp27, an LD-associated protein, is important in controlling LD size and lipid storage in adipocytes. In this paper, we demonstrate that Fsp27 is focally enriched at the LD–LD contacting site (LDCS). Photobleaching revealed the occurrence of lipid exchange between contacted LDs in wild-type adipocytes and Fsp27-overexpressing cells but not *Fsp27*-deficient adipocytes. Furthermore, live-cell imaging revealed a unique Fsp27-mediated LD growth process involving a directional net lipid transfer from the smaller to larger LDs at LDCSs, which is in accordance with the biophysical analysis of the internal pressure difference between the contacting LD pair. Thus, we have uncovered a novel molecular mechanism of LD growth mediated by Fsp27.

Introduction

Lipid droplets (LDs) are believed to originate from the ER and grow to a larger size by triacylglyceride (TAG) incorporation or by fusion of small LDs (Martin and Parton, 2006; Boström et al., 2007; Fei et al., 2008; Guo et al., 2008; Kadereit et al., 2008; Kuerschner et al., 2008; Bulankina et al., 2009; Farese and Walther, 2009; Stone et al., 2009; Walther and Farese, 2009; Murphy et al., 2010). However, molecular evidence for LD growth in a physiological condition is still lacking. Cell death–inducing DFF45-like effector (CIDE) family proteins, including Cidea, Cideb, and Fsp27/Cidec, are LD-associated proteins closely linked to the development of obesity, diabetes, and liver steatosis (Li et al., 2007; Matsusue et al., 2008; Puri et al., 2008; Qi et al., 2008; Rubio-Cabezas et al., 2009; Ye et al., 2009). Cidea and Fsp27 (Cidec)-defective adipocytes accumulate many small LDs (Zhou et al., 2003; Nishino et al., 2008; Toh et al., 2008; Rubio-Cabezas et al., 2009). Conversely, ectopic expression of Cidea and Fsp27 leads to the accumulation of larger LDs (Puri et al., 2007, 2008; Keller et al., 2008; Liu et al., 2009). Therefore, Fsp27 and Cidea play essential roles in controlling LD size in adipocytes.

Results and discussion

To understand the mechanism by which Fsp27 controls LD size in adipocytes, we analyzed the precise subcellular distribution of endogenous Fsp27 in differentiated 3T3-L1 adipocytes. Besides its localization to LD surface, Fsp27-positive staining was observed at the site where two LDs formed close contact in ∼30% (29 ± 5%) of adipocytes (Fig. 1 A). We defined this location as the LD–LD contacting site (LDCS). The percentage of cells with Fsp27 enrichment at LDCSs did not change significantly after oleic acid (OA) incubation or serum starvation (unpublished data). Untagged Fsp27 and Fsp27-GFP were also enriched at LDCSs when overexpressed (Fig. 1 B). LDCS enrichment of Fsp27-GFP was observed on LDs ranging from 0.2 to 5 µm without LD size preference (unpublished data). Cidea-GFP, a closely related family member, was also enriched

J. Gong and Z. Sun contributed equally to this paper.

Correspondence to Peng Li: li-peng@mail.tsinghua.edu.cn

Abbreviations used in this paper: ADRP, adipose differentiation–related protein; DIC, differential interference contrast; FA, fatty acid; LD, lipid droplet; LDCS, LD–LD contacting site; MEF, mouse embryonic fibroblast; MOI, mean optical intensity; OA, oleic acid; TAG, triacylglyceride; TLC, thin-layer chromatography.

The Rockefeller University Press $30.00
J. Cell Biol. Vol. 195 No. 6 953–963
www.jcb.org/cgi/doi/10.1083/jcb.201104142

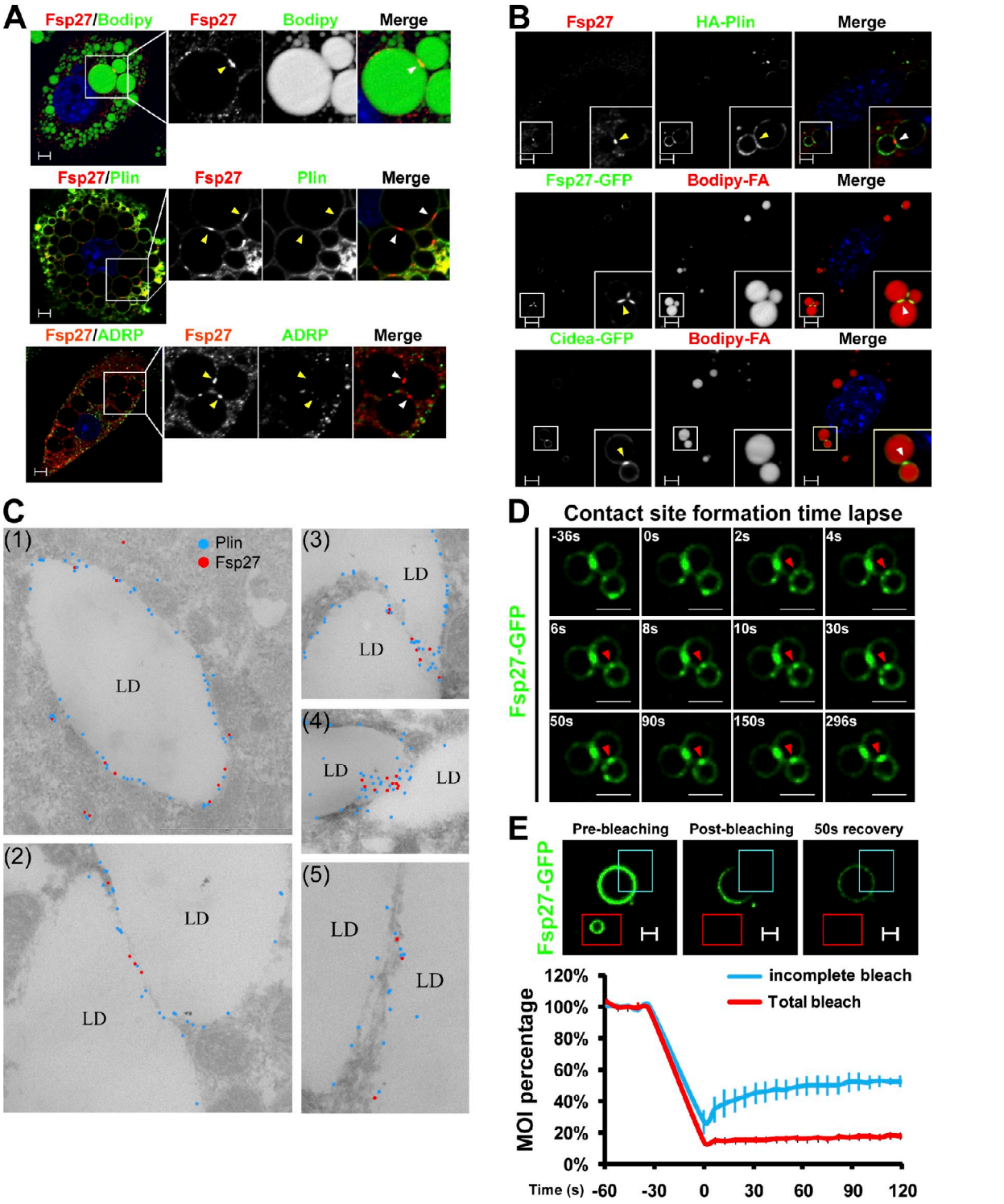

Figure 1. **Fsp27 is enriched at LDCS.** (A) Fsp27, but not Plin or ADRP, is enriched at the LDCS in 3T3-L1 adipocytes. The images on the right show the enlarged area of LDCSs in boxed areas on the left. (B) Untagged Fsp27 (coexpressed with HA-Plin), Fsp27-GFP, and Cidea-GFP are enriched at LDCSs when expressed in 3T3-L1 preadipocytes. Insets show enlargements of the boxed regions. (A and B) Arrowheads point to LDCSs. (C) Double immunogold labeling of Fsp27 and Plin in 3T3-L1 adipocytes by immuno-EM. (D) Images showing the kinetics of Fsp27-GFP enrichment at LDCSs. Red arrowheads point to the newly formed LDCS. (E) Fsp27 is rapidly diffused on the LD surface. Boxes represent photobleached areas. MOI in the bleached area was plotted as the percentage of the initial intensity from four independent experiments. Blue and red lines correspond to the intensity in blue or red boxed areas, respectively. Bars: (A and B) 5 µm; (C) 200 nm; (D) 4 µm; (E) 2 µm.

at the LDCS when overexpressed (Fig. 1 B). The enrichment at LDCSs was unique to Fsp27 and Cidea as Perilpin (Plin), and adipose differentiation–related protein (ADRP) in adipocytes showed no such enrichment, nor did several overexpressed LD-associated proteins (Plin, ADRP, TIP47, Rab18, and SNAP23; Figs. 1 A and S1 A). Double labeling of Fsp27 and Plin in

immunogold EM (immuno-EM) also confirmed an enrichment of Fsp27 at the sites where LDs were in close contact but a low density on the noncontacting area of LD surface (Figs. 1 C and S1 B). In contrast, Plin exhibited more uniform labeling over the entire LD surface (Figs. 1 C and S1 B). The enrichment of Fsp27 at LDCSs was also observed in isolated LDs and was well preserved after treatment with high salt (Fig. S1 C).

Live-cell imaging analysis demonstrated that LDs underwent rapid movement (Video 1). When two LDs began to contact with each other, Fsp27-GFP signal was first concentrated in the center of the contact site and then extended within the contact boundary, which took ∼5 min for completion (Fig. 1 D and Video 1). Furthermore, LDs tethered by LDCSs were able to comigrate, and the position of the LDCS on a given LD was mobile along the surface during LD movement (Fig. S1 D). No disassembly of Fsp27-LDCSs was observed within a 2-h observation period (Fig. S1 D), indicating that the LDCS is a stable structure.

Analysis of FRAP showed that Fsp27-GFP can undergo fast lateral diffusion on the LD surface, similar to that of GFP-Plin (Figs. 1 E and S1 E; Wang et al., 2009). However, the replenishing of Fsp27 or Plin from the cytosol or ER to LD surface was slow, as no fluorescent signal was recovered 5 min after the Fsp27-GFP or GFP-Plin signal on an entire LD was bleached (Figs. 1 E and S1 E). In contrast, the diffusion rate of Fsp27 from the LDCS to the surface of a noncontacting area or from one LD across the LDCS to its contact partner was slow (Fig. S1 F). A low recovery rate was also observed after Fsp27-GFP at LDCS was bleached, indicating that Fsp27 was sequestered at LDCSs after enrichment (Fig. S1 F). The rapid lateral diffusion of Fsp27 on the LD surface and the slow diffusion of Fsp27 from LDCSs to noncontacting areas may permit the rapid accumulation and stable enrichment of Fsp27 at LDCSs.

We then analyzed the structural requirements of Fsp27 for LDCS enrichment and promoting LD growth. The N-terminal region of Fsp27 (aa 1–135) was not localized to LDs and had no activity in promoting LD growth (Figs. 2 B and S2 A). Consistent with previous studies (Keller et al., 2008; Liu et al., 2009), the C-terminal region (aa 136–239) was able to associate with LDs, cluster at LDCSs, and promote LD growth (Fig. 2, A and B), albeit with lower activity (Fig. 2, D and E). Importantly, Fsp27 with further truncation in the C-terminal region (aa 172–239) showed no enrichment at LDCSs (Fig. 2, A and B) and had much lower activity to induce LD growth (Fig. 2, D and E). In addition, deletion of aa 179–217 (Δ179–217) on Fsp27 disrupted its LD localization and had no activity to induce LD growth (Fig. 2, A and B). Similar results were obtained for FLAG-tagged Fsp27 truncations (Fig. S2 B). We notice that although the majority of GFP-Fsp27 (172–239) was associated with LD surface (Fig. 2 A), as in the case of FLAG-Fsp27 (179–239; Fig. S2 B), broader GFP-Fsp27 (172–239) patch signal was observed in the proximity of some LDs. This may be a result of its high expression level or the relatively larger molecular mass of GFP than the short Fsp27 truncation. A chimeric protein consisting of aa 136–171 of Fsp27 fused to the LD-associated domain of AAM-B (aa 1–42; Zehmer et al., 2008) localized to LDs but was not enriched at LDCSs and had no activity (Figs. 2 [A and B] and S2 C). The expression levels of these truncations were similar (Fig. S2 D). These data indicate that the region of aa 179–217 is responsible for LD targeting, whereas aa 136–217 are required for enrichment at LDCSs. Importantly, enrichment at LDCSs is an a priori step for Fsp27 to exert its full activity in promoting LD growth.

Interestingly, we noted three conserved basic residues (K182, K186, and R190) in the region of aa 182–190 of Fsp27 that had a pattern of K/RyxxK/RyxxR (KKR motif; x represents the hydrophobic residue, and y represents the hydrophilic residue), representing a typical amphipathic α-helical structure (Fig. 2 C). Deletion of this region (Δ182–190) or substitution of all three basic residues with alanine (KKRA) abolished its LD-enlarging activity without affecting its association with LDs and enrichment at LDCSs (Figs. 2 and S2). Thus, these basic residues are crucial for Fsp27-dependent LD growth but are not required for LDCS enrichment.

Next, we performed FRAP analysis of neutral lipid dynamics in LD pairs with Fsp27 enrichment at LDCSs. When we bleached the red fluorescent lipid signal of LD1 and LD2 (Fig. 3 A, a), which were tethered by an LDCS, the signal remained low in LD1/2, and the signal of the nearby LD3 remained high 1 min after bleaching (Fig. 3 A, a–c). Interestingly, once LD3 formed an LDCS with LD2, the fluorescent signal in LD3 was reduced, accompanied by an increase in the fluorescent signal in LD1/2 (Fig. 3 A, d and e). Finally, the intensity of the fluorescent signals reached similar levels among these three LDs within 5 min (Fig. 3 A, d and e). These data indicate that the fluorescently labeled lipids in LD3 diffused into LD1/2. Reciprocally, when fluorescent signal in LD3 was bleached, fluorescent signal in LD1/2 diffused to LD3 (unpublished data). Therefore, fluorescently labeled lipids were exchanged bidirectionally via LDCSs, regardless of the LD size. Thin-layer chromatography (TLC) and liquid chromatography mass spectrometry analyses indicated that the majority of fluorescently labeled lipids in LDs of cells incubated with BODIPY-C12 fatty acids (FAs) corresponded to BODIPY-labeled TAGs (Fig. S3, A and B), indicating that lipids exchanging via Fsp27-positive LDCSs are TAGs. Lipid exchange was also observed via Cidea-GFP–enriched LDCS (unpublished data). The enrichment of Fsp27 and Cidea at LDCSs may recruit lipid transfer proteins or promote formation of a porelike structure at LDCSs, which allows neutral lipids to exchange among contacted LDs.

Quantitative analysis indicated that the lipid exchange rates between LDs connected by Fsp27-GFP– and Cidea-GFP–positive LDCSs were 0.13 ± 0.03 and 0.06 ± 0.02 $\mu m^3/s$, respectively (Fig. 3, B and C). Similar lipid exchange rates were obtained without illumination for GFP or by using untagged Fsp27 (Fig. 3, C and D), indicating that the induced lipid exchange is not a result of GFP-tag or photodamaging. Consistent with the slower lipid exchange rate, Cidea-GFP's activity in promoting LD growth was lower (Fig. 3, D and E). Interestingly, similar rates of lipid exchange (0.11 ± 0.02 $\mu m^3/s$) between LDs with Fsp27-postive LDCSs were also observed in PFA-fixed cells (Fig. S3 C). No lipid exchange was observed between LD pairs that had morphological contact but no Fsp27 enrichment at LDCSs (Figs. 3 F and S3 D) or among LD clusters in cells

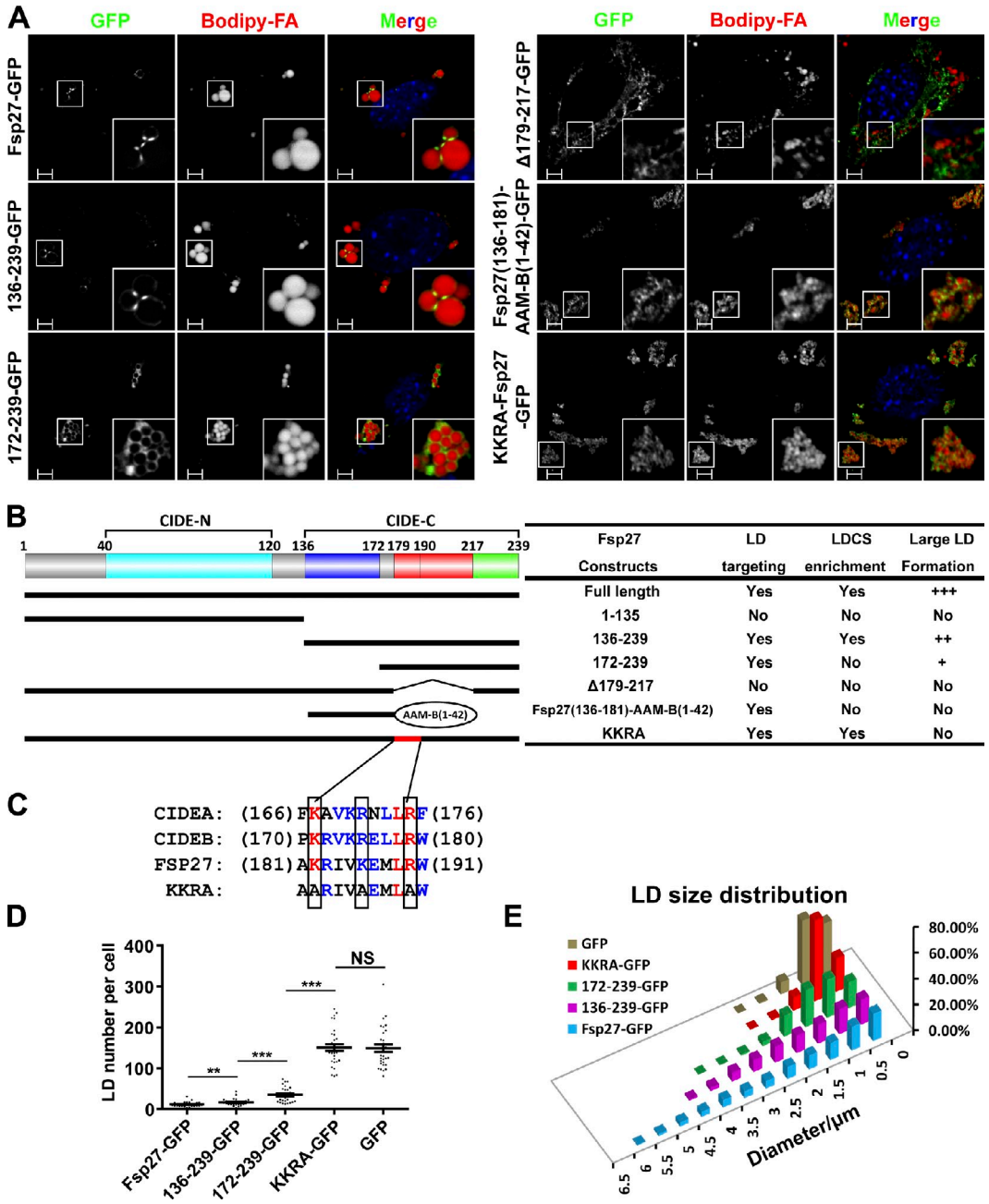

Figure 2. **Identification of regions on Fsp27 responsible for its LDCS enrichment and activity.** (A and B) Representative images (A) and a schematic diagram (B) showing the localization of Fsp27-GFP truncations and their activity to enlarge LDs in 3T3-L1 preadipocytes. Insets show enlargements of the boxed regions. CIDE-N and CIDE-C respectively refer to the evolutionary conserved domains at N- and C-terminal regions of CIDE family proteins. Bars, 5 µm. (C) Sequence alignment of aa 181–191 of Fsp27 with the corresponding region on Cidea and Cideb. Boxes highlight the conserved basic residues. KKRA represents substitutions of all three basic residues of Fsp27 with alanine. (D and E) LD number (D) and size distribution (E) in cells expressing Fsp27-GFP or its truncations. NS, no significant difference. **, $P < 0.01$; ***, $P < 0.001$. Data were collected from 30 GFP-positive cells in each group. Error bars represent SEM.

expressing GFP-Plin (Fig. 3 F and not depicted) or Fsp27-KKRA-GFP (Fig. S3 E). Therefore, Fsp27 enrichment at the LDCS is required for lipid exchange among contacted LDs, and the conserved basic residues in aa 182–190 are crucial for this activity.

Next, we assessed the in vivo role of Fsp27 in promoting neutral lipid exchange in mouse embryonic fibroblast (MEFs)–derived wild-type and *Fsp27*-deficient adipocytes and in 3T3-L1 adipocytes with an Fsp27 knockdown (Nian et al., 2010). FRAP analysis on randomly selected LDs that appeared to be contacting each other morphologically in wild-type MEF-derived adipocytes demonstrated that nearly half (36 out of 80) of these pairs underwent rapid neutral lipid exchange, with a rate of 5.66 ± 1.16 $\mu m^3/s$ (Fig. 3, F and G). Similar results were observed in 3T3-L1 adipocytes (Fig. 3 F). No lipid exchange was observed in LD clusters of *Fsp27*-deficient MEF-derived or Fsp27 knockdown 3T3-L1 adipocytes (Fig. 3, F and H). Overall, these data strongly indicate that Fsp27 acts as a crucial factor in

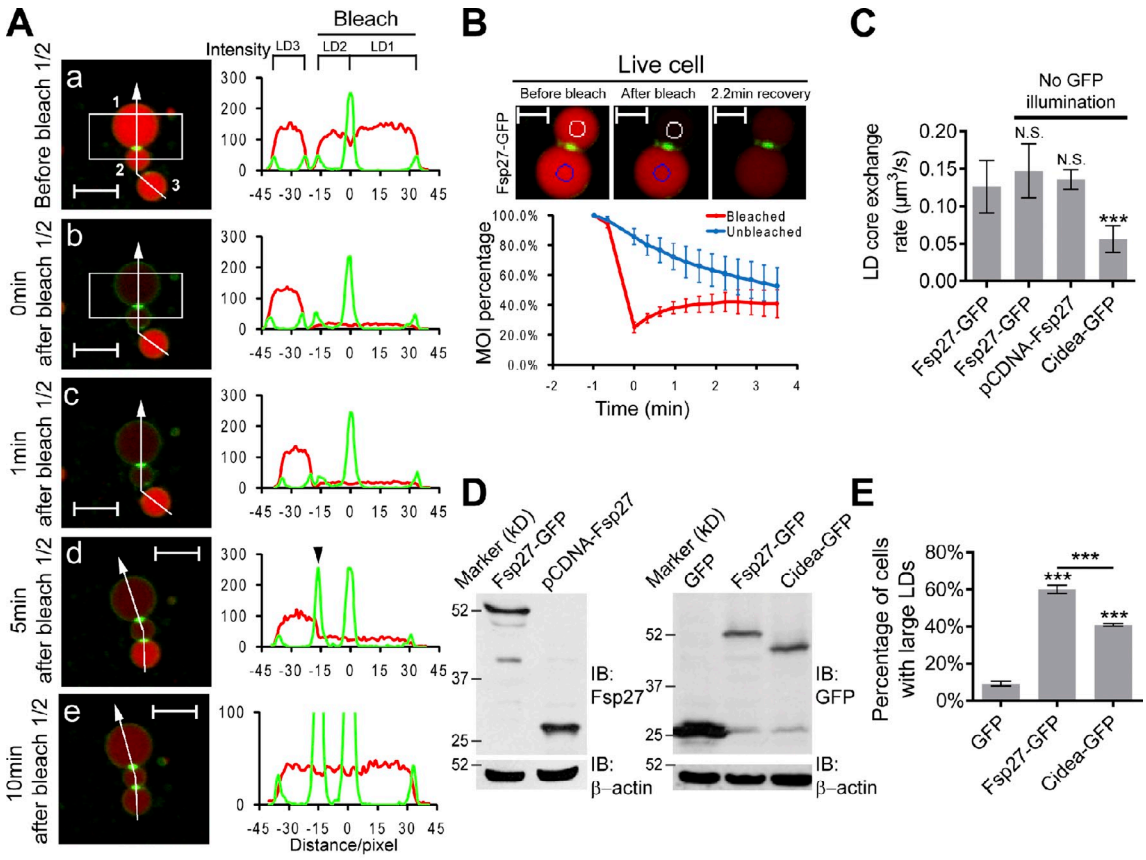

F

Cell Type	3T3-L1 preadipocyte			MEF-derived adipocyte		3T3-L1 adipocyte	
	GFP-Plin	Fsp27-GFP (enrichment at LDCS)		Wildtype	Fsp27-/-	Wildtype	siFsp27
		Yes	No				
LD pair/cluster with active lipid diffusion	0/20 (clusters)	50/50 (pairs)	0/20 (pairs)	36/80 (pairs)	0/80 (clusters)	42/80 (pairs)	0/80 (clusters)
Neutral lipid diffusion rate	0	0.13 ± 0.03 μm³/s	0	5.66 ± 1.16 μm³/s	0	5.40 ± 2.61 μm³/s	0

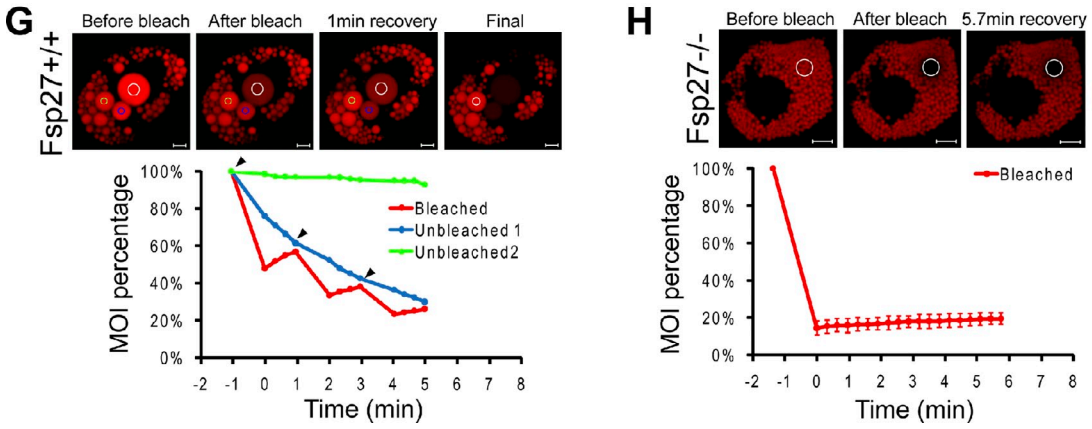

Figure 3. **Fsp27 promotes lipid exchange between contacted LDs.** (A and B) Fsp27 promotes lipid exchange between contacted LDs. (A) LD images in live 3T3-L1 preadipocytes expressing Fsp27-GFP were captured manually. 1, 2, and 3 (a) represent LD1, LD2, and LD3, respectively. The line profile at the right side of each image represents the fluorescent intensity of neutral lipids (red) and Fsp27-GFP (green) along the white arrow line. The black arrowhead (d) marks the newly formed LDCS between LD2 and LD3. The box represents the photobleached area. (B) MOI percentage in the bleached (white circle) or unbleached (blue circle) region was obtained from four independent experiments. (C) Lipid exchange rates in 3T3-L1 preadipocytes expressing Fsp27-GFP (with or without GFP illumination), untagged Fsp27, and Cidea-GFP. NS, no significant difference. ***, $P < 0.001$. At least six FRAP analysis data for each group were used for calculation. (D) Western blotting showing levels of GFP, Fsp27-GFP, untagged-Fsp27, and Cidea-GFP in C. IB, immunoblotting. (E) Quantitative analysis from three independent experiments showing the activity of Fsp27-GFP and Cidea-GFP to enlarge LDs in 3T3-L1 preadipocyte. A large LD is defined as an LD with a diameter ≥2.5 μm. (F) Lipid exchange activity in various cell types. Yes or No represent Fsp27 that is or is not enriched at LDCSs, respectively. 0/20 represents no active lipid diffusion in 20 LD pairs/clusters. siFsp27 represents Fsp27 knockdown 3T3-L1 adipocytes. (G and H) Lipid exchange in MEF-derived wild-type (*Fsp27*$^{+/+}$; G) and *Fsp27*-deficient (Fsp27$^{-/-}$; H) adipocytes. Photobleaching was repeated for three times, and arrowheads point to the starting point of each bleaching. White circles represent bleached regions. (B, C, E, and H) Error bars represent SD. Bars: (A, G, and H) 5 μm; (B) 2 μm.

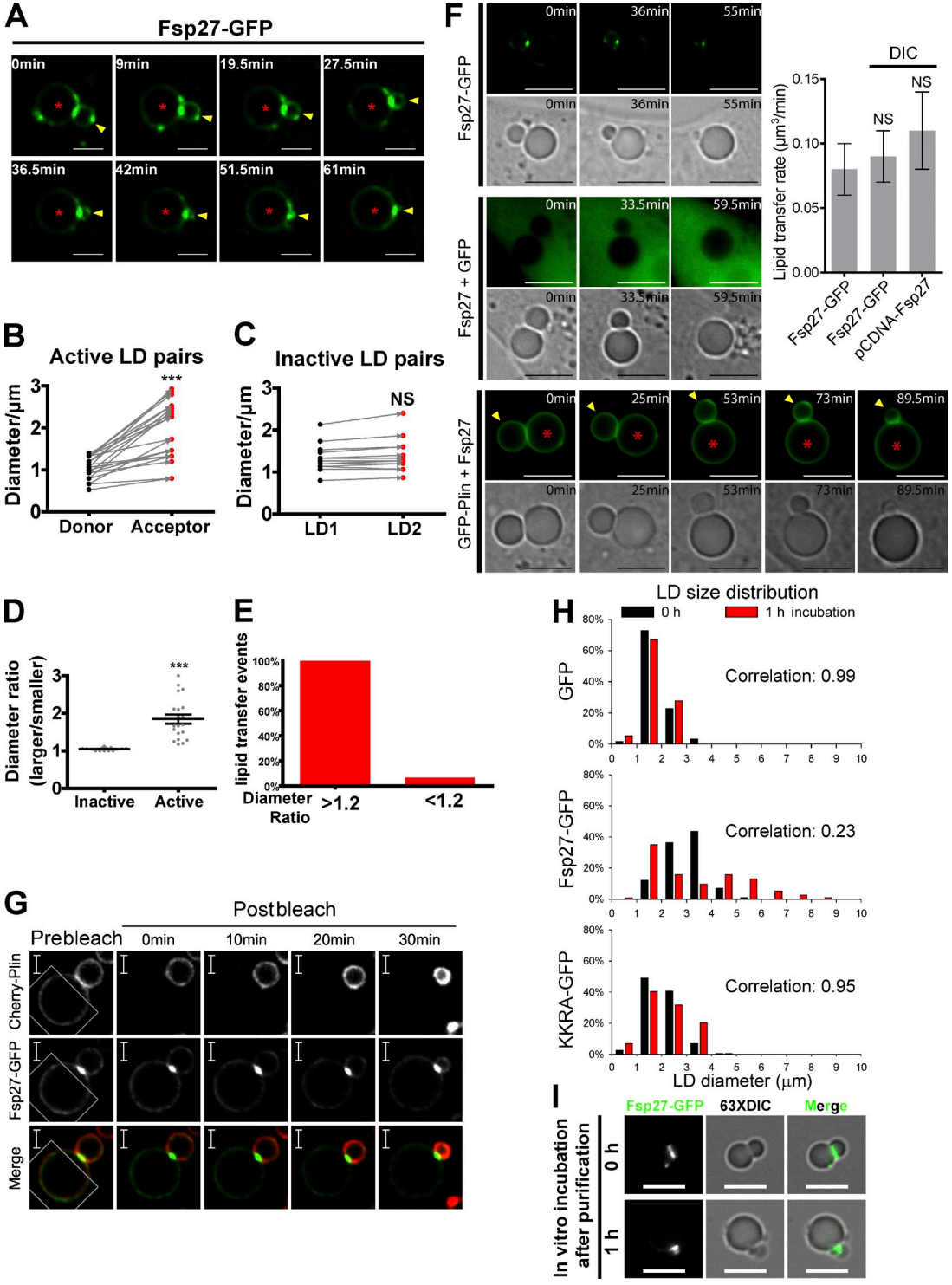

Figure 4. **Fsp27 promotes LD growth by mediating directional lipid transfer.** (A) Time-lapse images showing lipid transfer in 3T3-L1 preadipocytes expressing Fsp27-GFP. The red asterisks and yellow arrowheads represent the acceptor and donor LDs, respectively. (B–D) Size comparison of the donor and acceptor LDs of active (20 pairs) or inactive (15 pairs) lipid transfer pairs. Line arrows indicate contacted LD pairs. NS, no significant difference. ***, $P < 0.001$. Error bars in D represent SEM. (E) Based on data in D, the percentage of LD pairs with different diameter ratios that underwent active lipid transfer was calculated from 35 LD pairs out of 20 independent videos. (F) Time-lapse DIC images showing lipid transfer in 3T3-L1 preadipocytes expressing Fsp27-GFP and untagged Fsp27 (coexpressed with GFP or GFP-Plin). GFP images were taken in three or five key time frames. Arrowheads and asterisks represent the donor and acceptor contacted LD pair, respectively. Error bars represent SD. (G) The fate of Plin on smaller LDs during Fsp27-mediated lipid transfer. Cherry-Plin and Fsp27-GFP were coexpressed in 3T3-L1 preadipocytes. Cherry-Plin signal on the large LD was photobleached (boxed regions). (H) Fsp27 promotes lipid transfer and LD growth in vitro. Size distribution of LDs isolated from 293T cells expressing GFP, Fsp27-GFP, or Fsp27-KKRA-GFP before and after 1 h of incubation in vitro. Each distribution was calculated from 120–150 LDs. The experiment was repeated for three times, and a representative one is shown here. (I) Images of contacted LDs with Fsp27-GFP enrichment at the LDCS before and after incubation. Bars: (A) 4 μm; (F and I) 5 μm; (G) 2 μm.

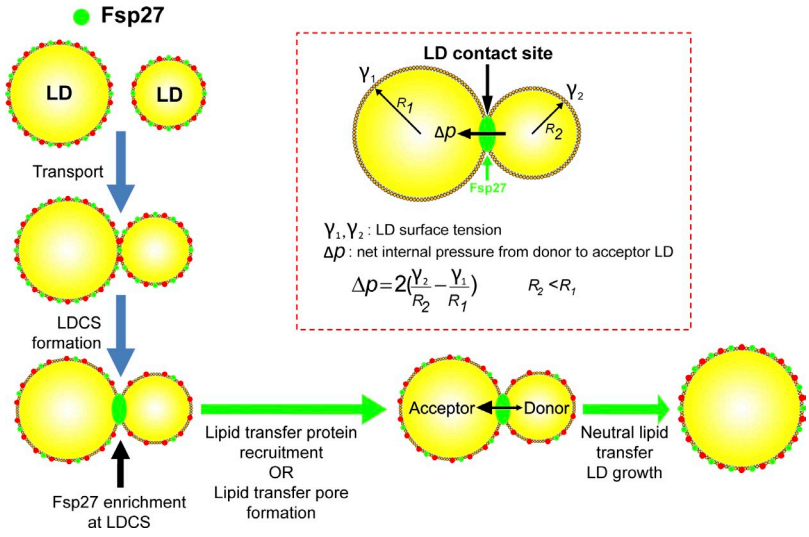

Figure 5. **Model depicting the mechanism of Fsp27-mediated LD growth.** An equation for the calculation of the internal pressure difference of contacted LDs is derived from Laplace's equation (see Materials and methods).

facilitating lipid exchange in adipocytes. However, it must be noted that the lipid exchange activity in adipocytes is 40-fold higher than in preadipocytes overexpressing Fsp27 (2.5-fold higher than endogenous protein levels in 3T3-L1 adipocytes). Thus, it is possible that additional adipocyte-specific factors synergistically enhance the function of Fsp27.

We then followed the fate of LD pairs with Fsp27 enrichment at LDCSs in live cells and observed that Fsp27 promoted LD growth by a unique lipid transfer process with several interesting features (Figs. 4 A and S3 F and Videos 2 and 3). First, lipid transfer occurred at LDCSs where Fsp27 was enriched. Second, Fsp27-GFP induced neutral lipid transfer from the smaller (donor) to the larger (acceptor) LD at a rate of 0.08 ± 0.02 μm^3/min. Finally, the smaller LD was gradually absorbed by the larger LD, leading to the growth of a larger LD. We observed that the donor LD was always smaller than the acceptor LD in 20 LD pairs undergoing active Fsp27-mediated lipid transfer (Fig. 4 B). Surprisingly, lipid transfer was not observed in some LD pairs with Fsp27-positive LDCSs (Fig. S1 D). The LD sizes in inactive pairs were similar, with a diameter ratio close to 1 (Fig. 4, C and D). Importantly, nearly 100% of LD pairs with a visible LDCS and a diameter ratio of ≥1.2 was actively transferring lipids, whereas only 7% of LD pairs that have a visible LDCS and a diameter ratio <1.2 was undergoing lipid transfer (Fig. 4 E). Therefore, the relative size of LDs in the contacted pair determines the lipid transfer status (active/inactive), with the larger LD as the acceptor and the smaller LD as the donor. Occasionally, we observed more than two LDs contacting each other and multiple lipid transfer events occurring simultaneously (Fig. S3 F and Video 3).

To eliminate possible artifacts as a result of photodamaging or GFP tagging, we followed lipid transfer process using differential interference contrast (DIC) microscopy. Fsp27-GFP or untagged Fsp27 induced active lipid transfer under DIC microscopy, at similar lipid transfer rates to that under GFP illumination (Figs. 4 F and S3 G and Videos 4–6). Further, lipid transfer processes were observed in cells expressing GFP-Plin and untagged Fsp27 under a DIC microscope (Fig. 4 F and Video 7). Similar lipid transfer processes were also observed in cells expressing Cidea-GFP (Fig. S3 H and Video 8) or untagged Cidea (not depicted). In contrast, no lipid transfer between LD pairs/clusters was observed in cells expressing GFP-Plin, GFP-ADRP, Fsp27-KKRA-GFP, or untagged Fsp27-KKRA under GFP illumination or a DIC microscope (Videos 9 and 10 and not depicted). Thus, Fsp27 or Cidea-mediated LD growth is not a result of GFP-tag or photodamage.

To examine the fate of LD-associated proteins on the small (donor) LD during Fsp27-mediated lipid transfer, we bleached the Cherry-Plin signal on the large (acceptor) LD of a contacted pair. 20 min after photobleaching, the donor LD became significantly smaller, indicating active lipid transfer within the pair (Fig. 4 G). Meanwhile, Cherry-Plin signal on the donor LD became condensed without redistributing to the surface of the large LD (Fig. 4 G). Therefore, Fsp27-mediated LD growth appears to be a unique process that involves a net lipid transfer from smaller to larger LDs via LDCSs but not diffusion and redistribution of LD-associated proteins from donor to acceptor LDs during the process.

To test whether Fsp27-dependent lipid transfer and LD growth could happen in vitro, we isolated LDs from cells expressing Fsp27-GFP and measured the sizes of LD pairs that had Fsp27 enrichment at LDCSs before and after 1 h of incubation in vitro (Fig. 4, H and I). A majority (73%) of isolated LDs had a diameter between 2 and 5 µm (Fig. 4 H). Strikingly, after a 1-h incubation, the number of LDs >5 µm increased (31% after incubation vs. 4% before incubation), which was accompanied by an increase in the number of small LDs with a size <2 µm (46% after incubation vs. 23% before incubation; Fig. 4 H). The populations of enlarging and shrinking LDs correlated with the acceptor and donors LDs, respectively (Fig. 4 I). The correlation coefficient was 0.23 for the LD size distribution before and after incubation, suggesting a different size distribution. Such a size change was not observed in LDs isolated from cells that expressed GFP or Fsp27-KKRA-GFP (Fig. 4 H). These data suggest that once Fsp27 is enriched at LDCSs, lipid transfer can continue in vitro in an autonomous or cytosolic factor–independent manner.

Overall, we have demonstrated that Fsp27 and Cidea are highly enriched at LDCSs and promote a directional lipid

transfer from smaller to larger LDs, resulting in the merging of contacted LDs (Fig. 5). The locally concentrated Fsp27 or Cidea at LDCSs may provide a tethering force for stable LD contact that is required for efficient lipid transfer. Alternatively, Fsp27 may cooperate with other factors to deform the phospholipid monolayer and trigger the formation of a specific junction pore or recruit lipid transfer proteins to allow lipid exchange and transfer between contacted LDs.

Directional net transfer of neutral lipids from smaller to larger LDs is a unique feature of Fsp27-mediated LD growth. This is probably a result of a higher internal pressure in the smaller LD, as it is inversely correlated with the size of LD according to Laplace's equation (Fig. 5). Under this scenario, once LDs contact each other and Fsp27 is enriched at an LDCS, a specific lipid transfer complex or channel could be formed to allow lipid content exchange (Fig. 5). Therefore, a critical step in Fsp27-mediated LD growth is the enrichment of Fsp27 at LDCSs. The mode of LD growth adopted by Fsp27 and Cidea is different from membrane fusion, as the former involves CIDE-mediated focal contact of pairing LDs and directional net lipid transfer between LDs with size disparity. Given that a truncation in human Cidec results in reduced LD size (Rubio-Cabezas et al., 2009) and that Cidea is also expressed in human adipocytes, it is likely that Fsp27 and Cidea also regulate LD growth in human adipocytes, perhaps in a cooperative manner.

Materials and methods

Plasmid DNA construction

Full-length cDNA encoding various LD-associated proteins (Plin, ADRP, TIP47, Rab18, SNAP23, DAGT2, and AAM-B) was cloned from cDNA of 8-d differentiated 3T3-L1 adipocytes and subcloned into pCMV5-HA, pCMV5-Flag, or pEGFP-C3 vectors. Full-length Cidea, truncation, or deletion fragments of Fsp27 that were amplified by PCR using appropriate primers from cDNA encoding full-length Cidea or Fsp27 were subcloned into XhoI–EcoRI sites of pCDNA-3.1(−) or pEGFP-N1 vectors or NdeI–XbaI sites of pCMV5-HA and pCMV5-Flag vectors. Amino acid substitutions on Fsp27 were generated by PCR site-directed mutagenesis from wild type–Fsp27-GFP. Chimera protein was constructed by fusing cDNA-encoding Fsp27 (aa 136–181) to aa 1–42 of AAM-B. The fidelity of all plasmid DNA constructs was verified by sequencing analysis.

Cell culture and transfection

293T cells and 3T3-L1 preadipocytes were cultured in DME (Invitrogen) containing 10% FBS (Invitrogen). Monolayers of 3T3-L1 preadipocytes were induced to differentiate into mature adipocytes, as previously described (Nian et al., 2010). In brief, cells were grown 2 d after confluence in DME/FBS and then in DME/FBS supplemented with 5 µg/ml insulin, 1 µM dexamethasone, and 0.5 mM isobutylmethylxanthine for an additional 2 d. The medium was then changed to DME/FBS supplemented with 5 µg/ml insulin. Cells were used for experiments 8 d after differentiation.

MEFs were isolated from 13.5-d wild-type and Fsp27-deficient mouse embryos, as previously described (Toh et al., 2008). Passage 2 of MEFs grown in coverslip-bottomed Lab-Tek chambers (Thermo Fisher Scientific) was used for differentiation. For the induction of MEFs to differentiate into adipocytes, MEFs were grown for 2 d after confluence and were then differentiated in DME/FBS supplemented with 8 µg/ml D-pantothenic acid, 8 µg/ml biotin, 1 µM dexamethasone, 0.5 mM isobutylmethylxanthine, 5 µg/ml insulin, and 1.0 µM pioglitazone (Taiyang Pharmaceutical Industry Co., Ltd.). 2 d later, the medium was changed to DME/FBS, 8 µg/ml D-pantothenic acid, 8 µg/ml biotin, 5 µg/ml insulin, and 1 µM pioglitazone. MEF-derived adipocytes were used for further experiments after 8 d of differentiation.

Plasmid DNAs were transfected into 293T cells and 3T3-L1 preadipocytes using Lipofectamine 2000 (Invitrogen), according to manufacturer's instruction, after cells were seeded for 12 h. To visualize clear LD morphology, transiently transfected 3T3-L1 preadipocytes were incubated with 200 µM OA complexed to albumin at a 6:1 molar ratio 5 h after transfection. BODIPY558/568 C12 (BODIPY-labeled FA; Invitrogen) was added into the medium at 1 µg/ml when needed. For live-cell time-lapse image analysis or FRAP, 3T3-L1 preadipocytes were grown in coverslip-bottomed Lab-Tek chambers (Thermo Fisher Scientific), transfected with indicated plasmids, and incubated with 200 µM OA. After 20 h, live cells were maintained on the microscopy stage in a temperature-, CO_2-, and humidity-controlled environment chamber and subjected to microscopy observation.

Lentivirus preparation and generation of stable cell lines

A DNA fragment encoding an siRNA specific for Fsp27 (5′-CTGTCTAGACAAAAAGGTCCAGGACATCTTGAAATCTCTTGAATTTCAAGATGTCCTGGACCGGGGATCTGTGGTCTCATACA-3′; Nian et al., 2010) was inserted into the FG12 expression vector (a gift from V. Tergaonkar, Institute of Molecular and Cell Biology, Singapore) and packaged into a lentivirus, as previously described (Dull et al., 1998). Lentivirus packaging and stable knockdown cell line generation were performed as previously described (Nian et al., 2010). In brief, 3T3-L1 preadipocytes were infected for 12 h with the lentivirus expressing the Fsp27-specific siRNA. Infection efficiency (>95%) was monitored by the signal of GFP, which is cointegrated into the genome with an siRNA expression module. After six passages, infected preadipocytes that stably expressed the siRNA were used as an Fsp27 knockdown cell line, and differentiation was induced. Western blot analysis showed knockdown efficiency is >90% (Nian et al., 2010). A lentivirus generated from the empty vector, which expressed only GFP, was used as the wild-type control (Fig. 3 F).

Immunofluorescent staining

Procedures for immunofluorescent staining were essentially the same as previously described (Toh et al., 2008). Cells were rinsed twice in PBS, fixed with 4% PFA (for 1 h), permeabilized with 0.1% saponin in PBS (for 30 min), blocked with 10% goat serum in PBS (for 1 h) followed by incubation with primary antibody (for 2 h), washed three times with PBS, and incubated with fluorescently labeled secondary antibody (1:500 dilution for 1 h) followed by Hoechst and/or BODIPY, as indicated. Coverslips were mounted after three times washing with PBS. Images for morphological analysis were acquired under an inverted microscope (Axiovert 200M; Carl Zeiss) with optical sectioning by an ApoTome module using a 63× oil immersion objective. Very high grid and averaging number 2 were used for optical sectioning.

3D reconstruction

3T3-L1 preadipocytes transfected with Fsp27-GFP were incubated with 200 µM OA and BODIPY-labeled FA for 15 h, fixed, and subjected to image analysis. Z stack images were acquired at 0.37 µm per section under an LSM710 microscope (Carl Zeiss).

Live-cell imaging

Live-cell imaging was performed on a spinning-disk confocal microscope (Revolution XD; Andor Technology) under a 60× oil immersion objective. To track the LD contact site formation, images were recorded as a 2-s time lapse. For lipid transfer process, images were recorded as a 30-s time lapse.

DIC microscope

DIC images were captured with an inverted microscope (Axiovert 200M) with a 100× oil objective. Acquisition was controlled under the MetaMorph software (Molecular Devices). Time-lapse videos were collected at 37°C with a 30-s interval over 1–2 h. At three to five key frames, one GFP channel picture was taken with epifluorescence (HBO 100 mercury vapor lamps; OSRAM) without interfering DIC time lapse.

Fsp27-immunolabeling EM

Immunolabeling EM experiments were performed according to published methods (Slot and Geuze, 2007). 8-d differentiated 3T3-L1 adipocytes were washed three times in serum-free medium and further incubated for 2 h before fixation in 2% PFA and 0.2% glutaraldehyde in isoosmotic phosphate buffer (pH 7.4). Cells were processed for frozen sectioning. Double labeling was performed with antibodies to Fsp27 and then 10 nm protein A gold followed by rabbit anti–perilipin A (P1998; Sigma-Aldrich) and 15 nm protein A gold with a glutaraldehyde blocking the step between.

FRAP

For FRAP analysis of protein dynamic on LDs in live cells, lipid-loaded 3T3-L1 preadipocytes that were transfected with indicated GFP constructs were used. Live cells were viewed under a confocal microscope (LSM710) using a 63× oil immersion objective. After five scanning images with a 6.25-s interval, selected regions were then bleached by 80 interactions at 100% laser power (489 diode laser) followed by time-lapse scanning images with a 6.25-s interval. MOI (mean optical intensity) of the region of interest was documented by the microscope automatically.

For FRAP-based lipid diffusion assay, 3T3-L1 preadipocytes transfected with indicated plasmids or MEF-derived adipocytes were incubated with 200 µM OA and BODIPY-labeled FA for 15 h and changed to fresh medium 1 h before the experiment. A confocal microscope (LSM710) with a 63× oil immersion objective was used. After three scanning images with a 19-s interval, selected regions were bleached by 500 interactions at 100% laser power (543 diode laser) followed by time-lapse scanning with a 19-s interval.

Procedures for FRAP analysis of lipid diffusion in fixed cells were similar to that in live cells, with minor modification. Cells were washed by PBS and fixed with 4% PFA for 2 h, rinsed three times in PBS, and sealed in mounting solution without permeablization. Experiments were performed at 25°C within 8 h after fixation.

For FRAP analysis, MOI values within the selected regions documented by microscope were used for calculation. To create fluorescence recovery curves, MOI values were transformed into 0–100% scales of the beginning signal and plotted using Excel (2007; Microsoft).

Image processing

All frames in the same time-lapse or FRAP experiments were adjusted in parallel in levels or contrast through Image-Pro (version 6.0; Media Cybernetics) or Zen (2009; Carl Zeiss) software. Images were exported out in 16-bit TIFF format. Further processing of single images (e.g., amplifying a certain region) was performed in Photoshop (CS2; Adobe). Videos were exported from Zen, and time stamps were incorporated by ImageJ (National Institutes of Health).

LD isolation and in vitro assay

For salt treatment, LDs were purified according to the method described by Liu et al. (2009), with minor modification (Bartz et al., 2007). In brief, lipid-loaded 293T cells transfected with Fsp27-GFP were harvested in PBS buffer containing 0.2 mM PMSF. Cell pellet was recovered by centrifugation at 500 *g* for 10 min and resuspended in 2 ml homogenization buffer (25 mM tricine, pH 7.6, 250 mM sucrose, and 0.2 mM PMSF). Cells were homogenized through Dounce homogenizer with loose pestle for 25 times. The postnuclear supernatant fraction after centrifugation at 1,000 *g* was laid with floating buffer (100 mM NaCl, 20 mM Hepes, pH 7.4, 0.2 mM PMSF, and 2 mM $MgCl_2$) and centrifuged at 200,000 *g* for 2 h. The floating fat cake was collected and resuspended in floating buffer in a 1.5-ml tube and centrifuged at 14,000 rpm for 5 min. The lower fraction was removed, and the upper LD fraction was further washed by floating buffer for three times. All procedures were performed at 4°C. Purified LDs were resuspended in 100 µl of floating buffer. 10 µl of LDs was gently mixed with 40 µl of floating buffer with 625 mM NaCl or 100 mM NaCl, respectively. The mixture was incubated on ice for 30 min. 10 µl of the mixture was then gently mixed with 20 µl of mounting solution and sealed under slips for microscopy observation.

Procedures for LD isolation used for protein localization analysis (Fig. S2 E), lipid analysis (Fig. S3, A and B), and in vitro lipid transfer assay (Fig. 4, H and I) were essentially the same as previously described (Joost and Schürmann, 2001), with minor modifications. Transfected HEK293T cells were washed once by PBS containing 0.2 mM PMSF and resuspended in TES buffer (20 mM Tris-HCl, 1 mM EDTA, 8.7% sucrose, pH 7.4, and 0.2 mM PMSF) and homogenized using Dounce homogenizer with loose pestle (30 strokes). After centrifugation at 8,000 *g* for 15 min, the supernatant was further centrifuged at 180,000 *g* for 2 h to pellet the ER fraction. Supernatant below the fat cake was collected and concentrated as a cytosol fraction. The upper fat cake was collected and resuspended in 6 ml TES buffer. 4 ml of floating buffer (100 mM NaCl, 20 mM Hepes, pH 7.4, and 0.2 mM PMSF) was laid onto it and centrifuged at 180,000 *g* for 2 h. The floating fat cake was collected and resuspended in floating buffer in a 1.5-ml tube and centrifuged at 14,000 rpm for 5 min. The lower fraction was removed, and the upper LD fraction was further washed by floating buffer for three times.

In vitro neutral lipid transfer and LD growth assay were performed as follows. 10 µl of LDs was gently mixed with 20 µl of mounting solution and sealed under coverslips before and after incubation at 37°C for 1 h. Image documentation was performed immediately and finished within 1 h. Diameters of LD pairs with clear Fsp27-GFP signal at LDCS before and after incubation were measured, and the diameter distributions were plotted.

Statistics

Data from at least three independent experiments were subjected to statistic analysis and plotted using Excel (2007) or Prism software (version 5.0; GraphPad Software). Results were reported either by mean ± SEM or mean ± SD, as indicated in the figure legends. Paired or unpaired (as indicated in the figure legends) two-tailed Student's *t* test was used for comparison.

Calculation of neutral lipid exchange rate via LDCS between contacted LDs

Neutral lipid exchange/diffusion via LDCS was assayed by measuring the intensity of fluorescently labeled neutral lipids after photobleaching. In brief, two LDs linked by one typical LDCS (marked by Fsp27-GFP enrichment) were selected. The neutral lipid core of one LD was photobleached, and the MOIs of both bleached and unbleached LD were documented. The rate of neutral lipid exchange per LDCS is defined as the volume of neutral lipid exchanged between two contacted LDs linked by only one LDCS in unit time. To calculate the neutral lipid diffusion rate, we have the following assumptions: (1) neutral lipid diffuses bidirectionally between two contacting LDs via LDCS; (2) neutral lipid diffusion is determined by the thermodynamic properties of neutral lipid molecules and the size of lipid diffusion pores or channel at LDCS; (3) the duration of FRAP assay is short (within 5 min), so the change in LD size as a result of net neutral lipid transfer from donor to acceptor LD is small and can be neglected; (4) the mean fluorescence intensity is linearly correlated with the actual concentration of fluorescent FAs within the measured region; and (5) neutral lipids diffuse rapidly inside LDs, and the rate of intra-LD diffusion is much higher than that of inter-LD diffusion. Thus, the mean fluorescence intensity reflects the concentration of fluorescent FAs of the measured LD.

Within a specific short duration (dt), the difference in lipid volume (dV) of neutral lipids diffuse via LDCS from LD1 to LD2. Meanwhile, dV of neutral lipids diffuse via LDCS from LD2 to LD1. The change of C_1 is dC_1:

$$dC_1 = \frac{dV(C_2 - C_1)}{V_1} = \frac{\varphi dt(C_2 - C_1)}{V_1}.$$

φ represents the neutral lipid exchange rate per LDCS. C represents the concentration of fluorescent FAs in LDs. I represents the MOI of the measured region. V represents the volume of total neutral lipids within one LD. t represents the time of the diffusion process. φ is a constant according to assumption 2. V is a constant according to assumption 3 and was calculated by measuring LD diameter in Zen. $I \propto C$ are constants according to assumptions 4 and 5.

$C_{1,0}$ and $C_{2,0}$ are initial concentrations of fluorescent FAs. As total fluorescent FA amount is constant within short duration after photobleaching, thus, $C_{2,0}V_2 + C_{1,0}V_1 = C_2V_2 + C_1V_1$.

Indeed, $C_2V_2 + C_1V_1$ only fluctuated within a ±5% range for the time points included in the calculation for each FRAP. Therefore,

$$\frac{dC_1}{dt} = \varphi\left[\left(\frac{C_{2,0}}{V_1} + \frac{C_{1,0}}{V_2}\right) - \left(\frac{1}{V_1} + \frac{1}{V_2}\right)C_1\right].$$

Because $I \propto C$,

$$\frac{dI_1}{dt} = \varphi\left[\left(\frac{I_{2,0}}{V_1} + \frac{I_{1,0}}{V_2}\right) - I_1\left(\frac{1}{V_1} + \frac{1}{V_2}\right)\right].$$

Both a and b are measurable constants, defined as

$$a = \frac{I_{2,0}}{V_1} + \frac{I_{1,0}}{V_2} \text{ and } b = \left(\frac{1}{V_1} + \frac{1}{V_2}\right).$$

Thus,

$$\varphi = \frac{dI_1}{(a - bI_1)dt} = \frac{dln(a - bI_1)}{-bdt}.$$

As we assume φ and b as constant, $ln(a - bI_1)$ and t are linearly correlated. Therefore, we performed linear fitting of $ln(a - bI_1)$ against t to calculate φ. Mean fluorescent intensity from three to six time points after each photobleaching was used for fittings. R^2 (correlation coefficient square) of all linear fittings was usually >0.9, indicating the validity of our assumptions and model. The neutral lipid exchange rate per LDCS was calculated as the mean value of the results calculated from both bleached and unbleached LDs.

Theoretical analysis of the physical basis for donor acceptor effect in Fsp27-mediated lipid transfer and LD growth process

We propose that the direction of net neutral lipid transfer via LDCS is determined by the internal pressure difference between contacted LDs. According to Laplace's equation in surface tension (Atkins and de Paula, 2002), the internal pressures of two LDs (designated as LD1 and LD2) could be calculated as follows:

$$p_{in1} = p_{out1} + \frac{2g_1}{r_1}$$

and

$$p_{in2} = p_{out2} + \frac{2\gamma_2}{r_2}$$

γ is the net surface tension between LD surface and cytosolic environment. r is the radius of LD. p_{out} and p_{in} represent the outside and internal pressure of LDs, respectively. Accordingly, smaller LD (smaller radius) tends to have higher internal pressure.

As contacted LD pairs reside in a similar cellular environment, thus, $p_{out1} = p_{out2}$. Therefore, the pressure difference at the pore or channel in LDCS is as follows:

$$\Delta p = p_{in1} - p_{in2} = 2\left(\frac{\gamma_1}{r_1} - \frac{\gamma_2}{r_2}\right).$$

As γ (surface tension) of LDs is determined by the physical and biochemical properties (density and composition of monolayer membrane and LD membrane–associated proteins) of LD surface, when LDs of contacted pairs have similar composition, the surface tension of two contacted LDs is similar to each other. Thus, $\gamma_1 = \gamma_2 = \gamma$ and

$$\Delta p = p_{in1} - p_{in2} = 2\gamma\left(\frac{1}{r_1} - \frac{1}{r_2}\right).$$

Therefore, neutral lipid gradually flows from the smaller LD (donor) to the larger LD (acceptor) when they are connected by LDCS. This is indeed the observation in Fig. 4 A and all documented LD transfer processes in live-cell imaging.

The rate of net neutral lipid transfer depends on internal pressure difference (Δp), recruitment of lipid transfer proteins, or the size of lipid transfer pores. Thus, Fsp27-mediated lipid transfer and LD growth could be regulated by directly modulating lipid transfer proteins recruitment or the size of pores generated and/or modulating LD surface tension by altering lipid and protein composition of LD surface.

Online supplemental material

Fig. S1 shows the characterization of LDCSs. Fig. S2 provides additional data on domain and mutation analysis to identify the region responsible for Fsp27 enrichment on the LDCS and its activity. Fig. S3 provides supporting data to prove that Fsp27 promotes neutral lipid exchange, net lipid transfer, and LD growth. Video 1 shows the kinetics of Fsp27-GFP enrichment at the LDCS. Videos 2–7 show Fsp27-induced lipid transfer processes. Video 8 shows Cidea-GFP–mediated lipid transfer. Videos 9 and 10 show that neither Fsp27-KKRA-GFP nor GFP-Plin induces lipid transfer. Online supplemental material is available at http://www.jcb.org/cgi/content/full/jcb.201104142/DC1.

We thank Drs. Li Yu and Lei Huang for assistance with imaging analysis.

This work was supported by grants from the National Basic Research Program of China (2007CB914404 and 2011CB910800) and the National Natural Science Foundation of China (30925017 and 31030038 to P. Li) and the Australian National Health and Medical Research Council (511005 to R.G. Parton).

Submitted: 29 April 2011
Accepted: 4 November 2011

References

Atkins, P.W., and J.C. de Paula. 2002. Atkins' Physical chemistry. Seventh edition. Oxford University Press, New York. 1149 pp.

Bartz, R., J.K. Zehmer, M. Zhu, Y. Chen, G. Serrero, Y. Zhao, and P. Liu. 2007. Dynamic activity of lipid droplets: Protein phosphorylation and GTP-mediated protein translocation. *J. Proteome Res.* 6:3256–3265. http://dx.doi.org/10.1021/pr070158j

Boström, P., L. Andersson, M. Rutberg, J. Perman, U. Lidberg, B.R. Johansson, J. Fernandez-Rodriguez, J. Ericson, T. Nilsson, J. Borén, and S.O. Olofsson. 2007. SNARE proteins mediate fusion between cytosolic lipid droplets and are implicated in insulin sensitivity. *Nat. Cell Biol.* 9:1286–1293. http://dx.doi.org/10.1038/ncb1648

Bulankina, A.V., A. Deggerich, D. Wenzel, K. Mutenda, J.G. Wittmann, M.G. Rudolph, K.N. Burger, and S. Höning. 2009. TIP47 functions in the biogenesis of lipid droplets. *J. Cell Biol.* 185:641–655. http://dx.doi.org/10.1083/jcb.200812042

Dull, T., R. Zufferey, M. Kelly, R.J. Mandel, M. Nguyen, D. Trono, and L. Naldini. 1998. A third-generation lentivirus vector with a conditional packaging system. *J. Virol.* 72:8463–8471.

Farese, R.V. Jr., and T.C. Walther. 2009. Lipid droplets finally get a little R-E-S-P-E-C-T. *Cell*. 139:855–860. http://dx.doi.org/10.1016/j.cell.2009.11.005

Fei, W., G. Shui, B. Gaeta, X. Du, L. Kuerschner, P. Li, A.J. Brown, M.R. Wenk, R.G. Parton, and H. Yang. 2008. Fld1p, a functional homologue of human seipin, regulates the size of lipid droplets in yeast. *J. Cell Biol.* 180:473–482. http://dx.doi.org/10.1083/jcb.200711136

Guo, Y., T.C. Walther, M. Rao, N. Stuurman, G. Goshima, K. Terayama, J.S. Wong, R.D. Vale, P. Walter, and R.V. Farese. 2008. Functional genomic screen reveals genes involved in lipid-droplet formation and utilization. *Nature*. 453:657–661. http://dx.doi.org/10.1038/nature06928

Joost, H.G., and A. Schürmann. 2001. Subcellular fractionation of adipocytes and 3T3-L1 cells. *Methods Mol. Biol.* 155:77–82.

Kadereit, B., P. Kumar, W.J. Wang, D. Miranda, E.L. Snapp, N. Severina, I. Torregroza, T. Evans, and D.L. Silver. 2008. Evolutionarily conserved gene family important for fat storage. *Proc. Natl. Acad. Sci. USA*. 105:94–99. http://dx.doi.org/10.1073/pnas.0708579105

Keller, P., J.T. Petrie, P. De Rose, I. Gerin, W.S. Wright, S.H. Chiang, A.R. Nielsen, C.P. Fischer, B.K. Pedersen, and O.A. MacDougald. 2008. Fat-specific protein 27 regulates storage of triacylglycerol. *J. Biol. Chem.* 283:14355–14365. http://dx.doi.org/10.1074/jbc.M708323200

Kuerschner, L., C. Moessinger, and C. Thiele. 2008. Imaging of lipid biosynthesis: How a neutral lipid enters lipid droplets. *Traffic*. 9:338–352. http://dx.doi.org/10.1111/j.1600-0854.2007.00689.x

Li, J.Z., J. Ye, B. Xue, J. Qi, J. Zhang, Z. Zhou, Q. Li, Z. Wen, and P. Li. 2007. Cideb regulates diet-induced obesity, liver steatosis, and insulin sensitivity by controlling lipogenesis and fatty acid oxidation. *Diabetes*. 56:2523–2532. http://dx.doi.org/10.2337/db07-0040

Liu, K., S. Zhou, J.Y. Kim, K. Tillison, D. Majors, D. Rearick, J.H. Lee, R.F. Fernandez-Boyanapalli, K. Barricklow, M.S. Houston, and C.M. Smas. 2009. Functional analysis of FSP27 protein regions for lipid droplet localization, caspase-dependent apoptosis, and dimerization with CIDEA. *Am. J. Physiol. Endocrinol. Metab.* 297:E1395–E1413. http://dx.doi.org/10.1152/ajpendo.00188.2009

Martin, S., and R.G. Parton. 2006. Lipid droplets: A unified view of a dynamic organelle. *Nat. Rev. Mol. Cell Biol.* 7:373–378. http://dx.doi.org/10.1038/nrm1912

Matsusue, K., T. Kusakabe, T. Noguchi, S. Takiguchi, T. Suzuki, S. Yamano, and F.J. Gonzalez. 2008. Hepatic steatosis in leptin-deficient mice is promoted by the PPARgamma target gene Fsp27. *Cell Metab.* 7:302–311. http://dx.doi.org/10.1016/j.cmet.2008.03.003

Murphy, S., S. Martin, and R.G. Parton. 2010. Quantitative analysis of lipid droplet fusion: Inefficient steady state fusion but rapid stimulation by chemical fusogens. *PLoS ONE*. 5:e15030. http://dx.doi.org/10.1371/journal.pone.0015030

Nian, Z., Z. Sun, L. Yu, S.Y. Toh, J. Sang, and P. Li. 2010. Fat-specific protein 27 undergoes ubiquitin-dependent degradation regulated by triacylglycerol synthesis and lipid droplet formation. *J. Biol. Chem.* 285:9604–9615. http://dx.doi.org/10.1074/jbc.M109.043786

Nishino, N., Y. Tamori, S. Tateya, T. Kawaguchi, T. Shibakusa, W. Mizunoya, K. Inoue, R. Kitazawa, S. Kitazawa, Y. Matsuki, et al. 2008. FSP27 contributes to efficient energy storage in murine white adipocytes by promoting the formation of unilocular lipid droplets. *J. Clin. Invest.* 118:2808–2821.

Puri, V., S. Konda, S. Ranjit, M. Aouadi, A. Chawla, M. Chouinard, A. Chakladar, and M.P. Czech. 2007. Fat-specific protein 27, a novel lipid droplet protein that enhances triglyceride storage. *J. Biol. Chem.* 282: 34213–34218. http://dx.doi.org/10.1074/jbc.M707404200

Puri, V., S. Ranjit, S. Konda, S.M. Nicoloro, J. Straubhaar, A. Chawla, M. Chouinard, C. Lin, A. Burkart, S. Corvera, et al. 2008. Cidea is associated with lipid droplets and insulin sensitivity in humans. *Proc. Natl. Acad. Sci. USA*. 105:7833–7838. http://dx.doi.org/10.1073/pnas.0802063105

Qi, J., J. Gong, T. Zhao, J. Zhao, P. Lam, J. Ye, J.Z. Li, J. Wu, H.M. Zhou, and P. Li. 2008. Downregulation of AMP-activated protein kinase by Cidea-mediated ubiquitination and degradation in brown adipose tissue. *EMBO J.* 27:1537–1548. http://dx.doi.org/10.1038/emboj.2008.92

Rubio-Cabezas, O., V. Puri, I. Murano, V. Saudek, R.K. Semple, S. Dash, C.S. Hyden, W. Bottomley, C. Vigouroux, J. Magré, et al. 2009. Partial lipodystrophy and insulin resistant diabetes in a patient with a homozygous nonsense mutation in CIDEC. *EMBO Mol Med*. 1:280–287. http://dx.doi.org/10.1002/emmm.200900037

Slot, J.W., and H.J. Geuze. 2007. Cryosectioning and immunolabeling. *Nat. Protoc.* 2:2480–2491. http://dx.doi.org/10.1038/nprot.2007.365

Stone, S.J., M.C. Levin, P. Zhou, J. Han, T.C. Walther, and R.V. Farese Jr. 2009. The endoplasmic reticulum enzyme DGAT2 is found in mitochondria-associated membranes and has a mitochondrial targeting signal that promotes its association with mitochondria. *J. Biol. Chem.* 284:5352–5361. http://dx.doi.org/10.1074/jbc.M805768200

Toh, S.Y., J. Gong, G. Du, J.Z. Li, S. Yang, J. Ye, H. Yao, Y. Zhang, B. Xue, Q. Li, et al. 2008. Up-regulation of mitochondrial activity and acquirement of brown adipose tissue-like property in the white adipose tissue of fsp27 deficient mice. *PLoS ONE.* 3:e2890. http://dx.doi.org/10.1371/journal.pone.0002890

Walther, T.C., and R.V. Farese Jr. 2009. The life of lipid droplets. *Biochim. Biophys. Acta*. 1791:459–466.

Wang, H., L. Hu, K. Dalen, H. Dorward, A. Marcinkiewicz, D. Russell, D. Gong, C. Londos, T. Yamaguchi, C. Holm, et al. 2009. Activation of hormone-sensitive lipase requires two steps, protein phosphorylation and binding to the PAT-1 domain of lipid droplet coat proteins. *J. Biol. Chem.* 284:32116–32125. http://dx.doi.org/10.1074/jbc.M109.006726

Ye, J., J.Z. Li, Y. Liu, X. Li, T. Yang, X. Ma, Q. Li, Z. Yao, and P. Li. 2009. Cideb, an ER- and lipid droplet-associated protein, mediates VLDL lipidation and maturation by interacting with apolipoprotein B. *Cell Metab.* 9:177–190. http://dx.doi.org/10.1016/j.cmet.2008.12.013

Zehmer, J.K., R. Bartz, P. Liu, and R.G. Anderson. 2008. Identification of a novel N-terminal hydrophobic sequence that targets proteins to lipid droplets. *J. Cell Sci.* 121:1852–1860. http://dx.doi.org/10.1242/jcs.012013

Zhou, Z., S. Yon Toh, Z. Chen, K. Guo, C.P. Ng, S. Ponniah, S.C. Lin, W. Hong, and P. Li. 2003. Cidea-deficient mice have lean phenotype and are resistant to obesity. *Nat. Genet.* 35:49–56. http://dx.doi.org/10.1038/ng1225